Chapter 8
Ultrafast Powder Diffraction

Andy Fitch and Caroline Curfs

Abstract An overview is given of the use of powder synchrotron-X-ray and neutron diffraction to study very fast physical or chemical processes that require time resolution of 500 ms or less. The experimental requirements to obtain data of good quality are considered, including the incident flux, detector characteristics, and the different strategies possible for irreversible and reversible processes. The latter are accessible via a stroboscopic approach whereas the former require the maximum rates of data acquisition. Some recent studies are described, drawn from the areas of combustion synthesis, metallurgy and catalysis. The exploitation of the bunch structure of a synchrotron ring to obtain time resolution in the sub-ns range with the pump-probe stroboscopic approach is also illustrated.

8.1 Introduction

An important use of powder diffraction is in the study of samples that are undergoing some sort of structural modification of a physical or chemical nature. Such experiments are often designed to investigate the kinetics and the mechanism of the process, which can be a phase transition caused by a change of the temperature, pressure or other external condition, or a chemical reaction taking place in the sample. Modern powder instruments, particularly at sources of penetrating radiation such as neutrons or high-energy synchrotron X-rays, allow sophisticated sample environments to be exploited, with great flexibility in the design of *in-situ* experiments to study evolving systems. The question naturally arises as to just how fast a process can be usefully measured.

A. Fitch (✉) • C. Curfs
ESRF, BP 220, F-38043 Grenoble Cedex, France
e-mail: fitch@esrf.fr; curfs@esrf.fr

U. Kolb et al. (eds.), *Uniting Electron Crystallography and Powder Diffraction*,
NATO Science for Peace and Security Series B: Physics and Biophysics,
DOI 10.1007/978-94-007-5580-2_8,

For measuring rapidly there are several technical issues to consider. For example, rapid processes require powder diffraction patterns to be recorded with appropriate time resolution – on the timescale of s, ms, μs, or faster still? – needing a detector system that can acquire data and be read out fast enough. However, simply registering patterns at enormous speed is of little use if the quality of the data is not sufficient to reveal the relevant details of the sample on that time scale. For the fastest, irreversible processes therefore, both high flux at the sample and efficient detectors are required. A high flux at the sample can be obtained by appropriate design of the source and instrumental optics, possibly focusing, and maximizing the energy spread of the radiation used to probe the sample.

For reversible processes, the stroboscopic approach can be used, in which the process under investigation is cycled and diffraction patterns registered during a small time window are accumulated over a number of cycles, progressively building up the statistical quality of the pattern. During the course of the experiment, the time window probes different parts of the cycle so as to cover it as required.

As a general rule, speed has to be traded against *d*-spacing or angular resolution. High resolution involves selecting only those neutrons or X-rays with an energy lying in a narrow range and whose trajectory from the source to the detector via the sample follows a stringently defined path (i.e. with a low divergence for the radiation incident on the sample and a tightly defined angular acceptance range for the detector, so as to have an exact measure of the Bragg angle θ). This necessarily excludes a large fraction of the photons or neutrons from the source or scattered by the sample which do not fulfill the criteria and so is a relatively inefficient process. Rapidly acquiring data of adequate statistical quality for meaningful analysis requires the maximum number of photons or neutrons to contribute to the diffraction pattern. Thus the selection criteria on the recorded radiation need to be relaxed by increasing the energy spread of the radiation and by allowing more pathways through the instrument (greater divergence), thus reducing the overall resolution.

8.2 Instrumentation

Fast data collection requires a fixed multi-channel detector system that can record the whole of the diffraction pattern essentially in one cycle. Scanning a detector system through the *d*-spacing range of interest necessarily takes a few seconds so is too slow to measure the fastest processes.

If working with monochromatic radiation and an angular-dispersive instrument then a fast-readout two-dimensional area detector or a one-dimensional position sensitive detector is the system of choice. 2-D detectors that have been found suitable for use with hard X-rays include the Frelon camera, based on CCD technology, and developed at the ESRF [1], and commercially available large flat-panel detectors, developed primarily for medical imaging at hard energies, which

have been exploited at speeds of up to 30 Hz [2–4]. A 1-D detector can be emulated by applying a mask to an area detector and only reading out the region of interest. Using the Frelon camera at beamline ID11 at ESRF, a time resolution of 10 ms has been achieved in this way with a 64×1 rebin of the data on the CCD chip [1]. Other read-out modes exist, such as rapidly transferring the electronic image to the masked part of the plate, which is read while the plate is re-exposed.

The best one-dimensional curved PSD for X-rays is the modular Mythen detector developed at the Paul-Scherrer Institute in Switzerland [5]. These detectors can be found on the powder diffraction beamlines at the Swiss Light Source, the Australian synchrotron, and Diamond in the UK. Based on Si technology, (at the time of writing), the detector is limited to detecting X-rays of up to $\approx$25 keV (0.5 Å wavelength). At SLS the detector covers 120° in 2θ, 30,720 channels, that can be read in parallel in 250 μs, with plans to be able to read even faster.

At ILL Grenoble, the angular-dispersive powder neutron diffractometer D20 [6] is equipped with a large curved microstrip PSD covering 153.6° in 2θ in 0.1° steps. The detector can be read in around 160 ms so giving a maximum time resolution of about 6 Hz. At ANSTO in Sydney, the high intensity powder diffractometer Wombat [7] is equipped with a similar curved PSD, covering 120° in steps of 0.125°. The detectors of both instruments can be used in stroboscopic mode.

With polychromatic radiation – which automatically exploits a greater fraction of the radiation from the source – the neutron time-of-flight approach is ideal, or for synchrotron radiation an energy-dispersive solid-state detector is required. Both methods work with detectors positioned at known 2θ angles that record the diffraction pattern by discriminating the wavelength or energy of each detected neutron or photon. For the fastest measuring rates multiple detectors are required. Examples of neutron powder diffractometers with extensive detector coverage are GEM [8] at ISIS, and the recently opened POWGEN [9] at the SNS (Oak Ridge). The former has a detector area of 7.27 m^2 covering scattering angles from 1.2° to 171.4°, and the latter, when completed, will have more than 40 m^2 of detectors from 10° to 170° 2θ (about 4 sr of detector coverage, some 240,000 individual elements).

With energy-dispersive measurements the detector consists of a liquid-nitrogen-cooled semiconducting Ge crystal. The energy of an absorbed X-ray photon, typically within the range 10–150 keV depending on the source, promotes electrons to the conduction band in proportion to its energy. By analyzing the amplitude of the charge pulses arriving from the crystal, the energy of the absorbed photon is determined with a multi-channel analyzer. The conversion from photon energy (in keV) to wavelength (in Å) is $E = 12.398/\lambda$ (where $12.398 \approx hc/e \times 10^7$). The energy resolution of such a detector is modest, around 2%. Owing to the need to take into account several energy-dependent effects, e.g. absorption and scattering factors, the shape of the incident X-ray spectrum, and the detector response, modeling the intensities of the powder diffraction pattern in a Rietveld refinement is generally difficult.

8.3 Examples

For the fastest processes, synchrotron radiation is generally expected to have the best performance, because of the very high flux from the source. However, neutrons, because of their penetrating power, can be used with larger samples, which can compensate to some extent.

8.4 Combustion Synthesis

This is a technique for synthesizing materials that exploits the high exothermic heat of reaction to promote a self-sustaining reaction, either by propagation from a point of ignition, or by heating the whole sample volume to a point where reaction occurs essentially simultaneously throughout. A number of advantages are cited for such an approach including reduced energy requirements, rapid reaction rates, and combined synthesis and sintering of the final product.

D20 at ILL was used at its peak-flux wavelength of 1.3 Å to investigate a number of systems by heating pre-pressed pellets of the starting products, 10–20 g, in a standard furnace for powder neutron diffraction until reaction was initiated [10–14]. Patterns were collected for 200–500 ms with readout of the detector requiring 80–400 ms. For the formation of Ti_3SiC_2 from a stoichiometric mixture of Ti, SiC and C five stages of the process were identified, including the transformation of α-Ti to β-Ti, the pre-ignition exothermic formation of intermediate TiC_x phases, the very rapid (sub-second) formation of a single intermediate phase, corresponding to a solid solution of Si in TiC. After an incubation period of a few seconds the product Ti_3SiC_2 nucleates and precipitates out as the temperature falls. Lattice parameter variations were used to estimate the bulk temperature and indicated that ≈2,600 K was attained. Rietveld analysis allowed the amount of each phase present to be determined, from which kinetic parameters were derived via a non-isothermal form of the Avrami equation. An activation energy of ≈45 kJ mol^{-1} was estimated for the nucleation and growth of the product phase. During cooling, the temperature deviated positively from an exponential decrease over a part of the range because of the release of latent heat correlated with the precipitation of the product phase. Analogous to differential thermal analysis, it was possible from this to estimate the enthalpy of formation of Ti_3SiC_2 as −76 kJ mol^{-1} [15].

On beamline ID11 at ESRF several systems have been studied in the self-propagating mode [1, 16–21]. Discs of the reactants were pressed, 20 mm in diameter × ≈2 mm thick, which were mounted in transmission with a 200 × 200 μm^2 monochromatic beam in the range 40–50 keV. The beam characteristics were chosen to obtain a balance between incident flux, penetration through the sample, the size of the combustion front, the grain size, and the angular resolution. Ignition via an electrically heated wire led to the propagation of the reaction through the sample at speeds of up to 100 mm s^{-1}, monitored with the 2-D Frelon camera with the temperature estimated via a pyrometer. The time resolution was typically in the

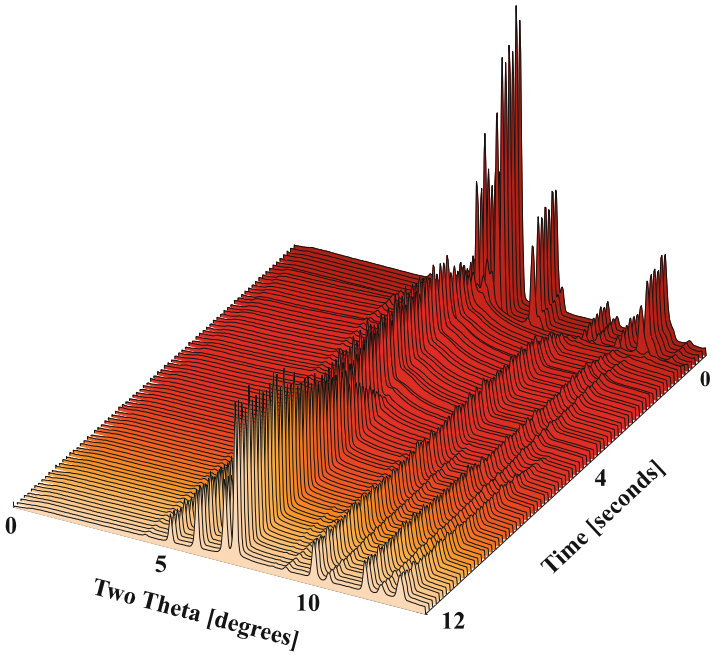

Fig. 8.1 Powder diffraction patterns of the Al-Ni-Ti-C system during self-propagating combustion synthesis measured on ID11 [17]

range 65–135 ms when exploiting the whole area of the detector and 20 ms when masking and rebinning on the chip as in the synthesis of Jacobsite, Fe_2MnO_4 [1]. Systems studied included the synthesis if TiC-NiAl (Fig. 8.1), TiC-WC and TiC-TiB_2 composites, Al-Ni intermetallics, TiC-FeTi cermets. For the TiC-NiAl system, for example, the formation of TiC accompanies the melting of Al then Ni and the formation of a (probably) ternary phase before the final formation of NiAl during cooling. The final product has small TiC particles embedded in a matrix of NiAl.

On beamline X11A at the NSLS Brookhaven the formation of several refractory carbides and diborides (of Ti, Zr, Nb, Hf or Ta) was studied in a specially built reaction chamber allowing operation under vacuum or in the presence of different reactive or inert gasses [22]. The chamber is equipped with a 2,048-channel 50-mm photodiode array covering 30° in 2θ, and a pyrometer. Data were collected in 50–200 ms at an energy of 8 keV in reflection mode.

Energy-dispersive measurements of the formation of barium, lithium and magnesium zinc ferrites were made on station 16.4 at the SRS Daresbury [23]. The reaction is driven by the oxidation of iron which is highly exothermic. Reaction was carried out in oxygen, and with the addition of sodium perchlorate as an internal oxidizing agent. Three energy-dispersive detectors were set at low 2θ angles of 1.8°, 4.7° and 7.5° and measurements were made in reflection with a 100 μm diameter white beam from the wiggler source. The time resolution was 100 ms. Measurements were

also made under an applied magnetic field using a 1.1 T permanent magnet with a cylindrical bore of 20 mm diameter. The X-ray beam direction was parallel to the axis of the bore and the fixed scattering geometry made the measurements possible. The magnetic field was seen to induce a transient phase identified as magnetite in the synthesis of barium ferrite.

8.5 Metallurgy

Processing of metals is an area where rapid changes of state are involved, such as during welding [24–28], heat treatment [29–32], and quenching [33, 34], etc. To understand the effects induced by these actions, detailed microscopic structural information is required.

At BL-10-2 at SSRL (Stamford), (beamline based on a multipole wiggler), rapid, *in-situ* powder diffraction patterns were recorded as gas tungsten arc spot welds were made on carbon-manganese steel bars [24, 25]. To prevent oxidation the experiments were performed under a helium atmosphere, and used a 50-mm photodiode array covering 24–54° 2θ with a time resolution of 100 ms (260 μm X-ray spot) or 50 ms (730 μm spot size) at an X-ray energy of 12.0 keV. The fcc-to-bcc ($\gamma \rightarrow \alpha$) transition on cooling happened twice as fast as the bcc-to-fcc ($\alpha \rightarrow \gamma$) transition on heating reflecting, most probably, differences in the heating and cooling rates. Subtle changes in *d*-spacings indicated the precipitation of carbide or the relief of residual stress during heating. Detailed analysis indicated that there were differences in microstructure between the weld fusion zone and the nearby heat-affected zone (HAZ). The same experimental arrangement was also used to study welding of stainless steel at two positions in the HAZ, 0.2 and 0.7 mm from the fusion zone boundary, to investigate the transformation of austenite (γ phase) to ferrite (δ phase) on heating, and back on cooling [26]. Volume fractions, peak positions and widths were tracked and correlated with the temperature calculated via a numerical heat transfer and fluid flow model.

Time resolution of down to 10 ms was exploited at Spring-8 (Japan) using undulator beamline 46XU to study solidification during welding of martensitic steel using X-rays of energies 18 or 30 keV and a large area pixel detector [28]. In a further development, fast diffraction measurements during heat treatment of mild steel and low-temperature transformation steel were combined with concurrent fast laser scanning confocal microscopy, allowing insight into the origin and morphology of the observed microstructural changes accompanying phase transitions on cooling [29].

NiTi shape memory alloy wires must be annealed, modifying the cold-worked deformed microstructure, and mechanically constrained to set the wire, to give the shape-memory properties. Practically, heating can be done via an electrical pulse. ID11 was used to study the transformation of a wire under rapid electrical heating with applied tensile force and simultaneous electrical resistivity measurements [32]. By masking the detector and rebinning on the chip, a time resolution of 10 ms

was obtained. Marked changes in microstructure and strain were apparent from monitoring the evolution of the 011 reflection of the austenitic phase present, depending on the power dissipated during the thermal treatment.

8.6 Catalysis

Many chemical processes are catalyzed by metallic nanoparticles such as platinum or gold. Studying such systems by conventional diffraction is hampered because of the effect of particle-size broadening on the diffraction pattern. Nevertheless the structure of such systems can be studied by measuring to high Q values (where $Q = 4\pi \sin\theta/\lambda$), then Fourier transforming to give the pair distribution function (PDF). Measuring to high Q requires hard X-ray energies and, if not scanning to high 2θ, a large 2-D detector such as the GE medical imaging detector [3, 4] installed at the APS (Illinois), which moreover has a time resolution of 30 Hz. Thus the reduction of PtO_2 to Pt metal by hydrogen at 200°C was studied at an energy of 77 keV (just below the Pt K edge to minimize fluorescence) while recording data up to $\approx$25 $Å^{-1}$. The individual patterns collected in 130 ms could be suitably converted to yield a PDF showing the overall course of the reaction. In a similar experiment, catalytic Pt nanoparticles were prepared in situ by reducing with hydrogen a deposit of H_2PtCl_6 on a TiO_2 support [35]. The support forms the bulk of the system, but nevertheless sensitivity to the Pt particles is achieved by adopting the differential PDF approach whereby the PDF of the bare support (measured under equivalent conditions) is subtracted from the total PDFs obtained from the individual patterns. It is evident that the reduction follows pseudo-zero-order kinetics, and by performing the measurements at different temperatures (100, 150 and 200°C) an Arrhenius plot allows an activation energy for the reduction of a nanoparticle to be estimated at about 50 kJ mol^{-1}, a quantity very difficult to obtain by any other means.

At ESRF beamline ID15B diffraction patterns from 2% of Pd nanoparticles ($\approx$3 nm diameter) supported on alumina were recorded using high energy (86.8 keV) X-rays with a time resolution of 2 Hz [36]. During the measurements the atmosphere was cycled between CO and NO, in simulation of a working car exhaust catalyst. The reactions were also monitored by diffuse reflectance infrared spectroscopy (DRIFTS) and mass spectroscopy (MS) of the effluent gas. A complementary experiment applied time resolved dispersive EXAFS at the Pd K edge in combination with DRIFTS and MS. During the CO cycle the Pd cell parameter was seen to increase linearly with time accompanied by the production of CO_2 then reverse when switched to NO flow. The studies show that CO dissociates on the surface of the nanoparticles to produce CO_2 and PdC_x (lattice expansion consistent with $x \leq 0.06$). Under NO, the PdC_x is converted back to Pd, with the emission of CO_2 and nitrogen gas. The IR spectroscopic measurements indicate moreover that the formation of the PdC_x also promotes the adsorption of CO in a linear configuration (PdCO) compared to a bridging (Pd_2CO) arrangement.

8.7 Stroboscopic Measurements

Commercial, doped, polycrystalline lead zirconate titanate (PZT) piezoelectric ceramics were measured in a cyclic electric field of ± 400 V mm^{-1} at frequencies up to 500 Hz via the stroboscopic approach using WOMBAT [37]. Each detected neutron is time stamped and subsequently binned together with others that have been scattered from the sample at the equivalent time in the electrical cycle. The data resulting from the sum of many cycles can be represented relative to just a single cycle. An effective time resolution of 30 μs is available using this approach. Shifts in peak positions indicate the level of piezoelectric strain generated by the field and showed no dependence on frequency. Time-of-flight neutron diffraction studies performed at ISIS on a related system using ENGIN-X [38] showed time and orientation dependence of the lattice strains [39]. Possible mechanisms for the observed behavior were discussed.

Rather than using the detector to time the arrival of the scattered radiation, the source can be pulsed to give the time frame for stroboscopic measurements. This is particularly appropriate at a synchrotron where tight bunches of electrons are in fact circulating in the storage ring. Specific ring-filling modes can be exploited to enhance the possibilities for time-resolved studies. Thus at ESRF, when operating in 16-bunch mode, an intense pulse (70 ps duration) of X-rays is emitted from the ring every 180 ns as each bunch of electrons flashes past the entrance to a beamline. A high-speed chopper in the X-ray beam can be used to select the source frequency desired for any particular experiment. Of particular note are pump-probe experiments, whereby a very short laser pulse (of the order 100 fs) excites the sample, which is then probed with an X-ray pulse a chosen delay time later. The diffraction pattern can be simply accumulated over a number of cycles on a passive 2-D detector like an image plate, because of the intrinsic low dark current for these devices. Accurate electronics are required to synchronize the laser and chopper with the bunch clock tracking the electron bunches in the storage ring.

Two examples studied at the ESRF on beamline ID09B are 4-(dimethylamino) benzonitrile and 4-(diisopropylamino)benzonitrile [40, 41], whose fluorescence properties indicate that photo-excitation leads to the formation of an intramolecular charge-transfer state. Powder diffraction patterns were collected over 10 min at a frequency of 897 Hz at delay times ranging from -150 ps (i.e. as a reference before the laser excitation) to 2,500 ps after excitation. Only about 5% of the molecules are excited by the laser, so the diffraction pattern is from a structure containing both excited and ground-state molecules. Rietveld refinement of the structure from the diffraction patterns gave the number of excited (distorted) molecules as a function of delay time, and the nature of the molecular change induced by the photo-excitation. For the isopropyl analogue, an exponential decay time of 6.3 (± 2.8) ns was observed for the excited molecules (compared to 3.28 ns seen spectroscopically). The main distortion to the molecules was a change in the torsion angle between the diisopropylamino group and the benzene ring from 13° to 14° determined from the pre-excitation patterns (14.3° in the single-crystal structure) to 10 (± 1–2)°.

Such experiments give the highest time resolution currently possible for powder diffraction experiments, though future experiments using free-electron lasers are being considered [42].

8.8 Data Analysis

Measuring data at high speed produces a large number of powder patterns that need to be analyzed, to extract lattice parameters, phase fractions, structural parameters, etc. as required to understand the behavior of the system. Modern Rietveld refinement programs (e.g. GSAS, Fullprof, Topas) allow a series of patterns to be processed. One approach takes the output from pattern n as the input to pattern $n + 1$, sequentially progressing through the series, (but watch out for abrupt changes as the system evolves). Another way is to analyze several datasets simultaneously in a single refinement, tying together chosen parameters between patterns so as to vary according to an underlying theoretical model or to follow an empirical evolution, i.e. essentially fitting to a data surface rather than to the individual patterns [43]. For example, instead of refining the lattice parameters for each pattern, the thermal expansion coefficients can be refined, defining how the lattice parameters vary over the series. Care is required in analyzing patterns from time-resolved measurements as they are necessarily compromised by the need to measure rapidly. However you choose to analyze your data, good luck.

References

1. Labiche JC et al (2007) The fast readout low noise camera as a versatile X-ray detector for time resolved dispersive EXAFS and diffraction studies of dynamic problems in materials science, chemistry and catalysis. Rev Sci Instrum 78:091301
2. Daniels JE, Drakopoulos M (2009) High-energy X-ray diffraction using the Pixium 4700 flat-panel detector. J Synchrotron Radiat 16:463–468
3. Chupas PJ, Chapman KW, Lee PL (2007) Applications of an amorphous silicon-based area detector for high-resolution, high-sensitivity and fast time-resolved pair distribution function measurements. J Appl Crystallogr 40:463–470
4. Lee JH et al (2008) Synchrotron applications of an amorphous silicon flat-panel detector. J Synchrotron Radiat 15:477–488
5. Bergamaschi A et al (2010) The MYTHEN detector for X-ray powder diffraction experiments at the Swiss Light Source. J Synchrotron Radiat 17:653–668
6. Hansen TC, Henry PF, Fischer HE, Torregrossa J, Convert P (2008) The D20 instrument at the ILL: a versatile high-intensity two-axis neutron diffractometer. Meas Sci Technol 19:034001
7. Studer AJ, Hagen ME, Noakes TJ (2006) Wombat: the high-intensity powder diffractometer at the OPAL reactor. Physica B 385–386:1013–1015
8. Hannon AC (2005) Results on disordered materials from the GEneral Materials diffractometer, GEM, at ISIS. Nucl Instrum Method A 551:88–107
9. http://www.jcns.info/POWGEN

10. Riley DP, Kisi EH, Wu E, Hansen T, Henry P (2010) Applications of in situ neutron diffraction to optimisation of novel materials synthesis. Studying kinetics with neutrons, Springer Series in solid state sciences, vol 161. Springer, Berlin/Heidelberg, pp 123–148
11. Kisi EH, Riley DP (2003) Neutron diffraction studies of self-propagating high-temperature synthesis. IUCr Comm Powder Diffr Newsl 29:18–20
12. Riley DP, Kisi EH, Hansen TC, Hewat AW (2002) Self-propagating high-temperature synthesis of Ti3SiC2: I, ultra-high-speed neutron diffraction study of the reaction mechanism. J Am Ceram Soc 85:2417–2424
13. Kisi EH, Riley DP, Curfs C (2006) Ultra-high speed neutron diffraction studies of combustion synthesis. Physica B 385–386:487–492
14. Riley DP, Kisi EH, Hansen TC (2008) Self-propagating high-temperature synthesis of Ti3SiC2: II. Kinetics of ultra-high-speed reactions from in situ neutron diffraction. J Am Ceram Soc 91:3207–3210
15. Kisi EH, Riley DP (2002) Diffraction thermometry and differential thermal analysis. J Appl Crystallogr 35:664–668
16. Curfs C, CanoI G, Vaughan GBM, Rodríguez MA, Turillas X, Kvick A (2000) Intermetallic-ceramic composites synthesis by SHS. Time-resolved studies using synchrotron radiation X-rays. Int J SHS 9:331–339
17. Curfs C, Cano IG, Vaughan GBM, Turillas X, Kvick A, Rodríguez MA (2002) TiC-NiAl composites obtained by SHS: a time-resolved XRD study. J Eur Ceram Soc 22:1039–1044
18. Contreras L, Turillas X, Vaughan GBM, Kvick A, Rodríguez MA (2004) Time-resolved XRD study of TiC-TiB2 composites by SHS. Acta Mater 52:4783–4790
19. Contreras L, Turillas X, Mas-Guindal MJ, Vaughan GBM, Kvick A, Rodríguez MA (2005) Synchrotron diffraction studies of TiC/FeTi cermets obtained by SHS. J Solid State Chem 178:1595–1600
20. Mas-Guindal MJ, Contreras L, Turillas X, Vaughan GBM, Kvick A, Rodríguez MA (2006) Self-propagating high-temperature synthesis of TiC-WC composite materials. J Alloys Compd 419:227–233
21. Curfs C, Turillas X, Vaughan GBM, Terry AE, Kvick A, Rodríguez MA (2007) Al-Ni intermetallics obtained by SHS; A time-resolved X-ray diffraction study. Intermetallics 15:1163–1171
22. Wong J, Larson EM, Waide PA, Frahm R (2006) Combustion front dynamics in the combustion synthesis of refractory metal carbides and di-borides using time-resolved X-ray diffraction. J Synchrotron Radiat 13:326–335
23. Parkin IP, Pankhurst QA, Affleck L, Aguas MD, Kuznetsov MV (2001) Self-propagating high temperature synthesis of BaFe12O19, Mg0.5Zn0.5Fe2O4 and Li0.5Fe2.5O4; time resolved X-ray diffraction studies (TRXRD). J Mater Chem 11:193–199
24. Wong J (2003) Phase mapping and transformation dynamics in fusion welds. IUCr Comm Powder Diffr Newsl 29:26–30
25. Wong J, Ressler T, Elmer JW (2003) Dynamics of phase transformations and microstructure evolution in carbon-manganese steel arc welds using time-resolved synchrotron X-ray diffraction. J Synchrotron Radiat 10:154–167
26. Palmer TA, Elmer JW, Babu SS (2004) Observation of ferrite/austenite transformations in the heat affected zone of 2205 duplex stainless steel spot welds using time resolved X-ray diffraction. Mater Sci Eng A 374:307–321
27. Stone HJ, Bhadeshia HKDH, Withers PJ (2008) In situ monitoring of weld transformations to control weld residual stresses. Mater Sci Forum 571–572:393–398
28. Komizo Y, Terasaki H (2010) In-situ observation of solidification behavior during welding. Mater Sci Forum 638–642:3722–3726
29. Terasaki H, Komizo Y (2011) Diffusional and displacive transformation behavior in low carbon-low alloy steels studied by a hybrid in situ observation system. Scr Mater 64:29–32
30. Elmer JW, Palmer TA, Specht ED (2007) In situ observation of sigma phase dissolution in 2205 duplex stainless steel using synchrotron X-ray diffraction. Mater Sci Eng A 459:151–155

31. Zhang D, Terasaki H, Komizo Y (2009) In situ observation of phase transformation in Fe-0.15C binary alloy. J Alloys Compd 484:929–933
32. Malard B, Pilch J, Sittner P, Delville R, Curfs C (2011) In situ investigation of the fast microstructure evolution during electropulse treatment of cold drawn NiTi wires. Acta Mater 59:1542–1556
33. Epp J, Hirsch T, Curfs C (2012) In situ X-Ray diffraction analysis of unexpected carbon partitioning during quenching of low carbon steel. Metall Mater Trans A 43:2210–2217
34. Epp J, Hirsch T, Kuznetsov A, Curfs C Martensite self-tempering in a ball bearing steel: in situ X-ray diffraction analysis during quenching (in preparation)
35. Chupas PJ, Chapman KW, Jennings G, Lee PL, Grey CP (2007) Watching nanoparticles grow: the mechanism and kinetics for the formation of TiO2-supported platinum nanoparticles. J Am Chem Soc 129:13822–13824
36. Newton MA, Michiel MD, Kubacka A, Fernández-García M (2010) Combining time-resolved hard X-ray diffraction and diffuse reflectance infrared spectroscopy to illuminate CO dissociation and transient carbon storage by supported Pd nanoparticles during CO/NO cycling. J Am Chem Soc 132:4540–4541
37. Pramanick A et al (2010) In situ neutron diffraction studies of a commercial, soft lead zirconatetitanate ceramic: response to electric fields and mechanical stress. Appl Phys A 99:557–564
38. Santisteban JR, Daymond MR, James JA, Edwards L (2006) ENGIN-X: a third-generation neutron strain scanner. J Appl Crystallogr 39:812–825
39. Jones JL et al (2007) Time-resolved and orientation-dependent electric-field-induced strains in lead zirconatetitanate ceramics. Appl Phys Lett 90:172909
40. Davaasambuu J, Durand P, Techert S (2004) Experimental requirements for light-induced reactions. J Synchrotron Radiat 11:483–489
41. Techert S, Zachariasse KA (2004) Structure determination of the intramolecular charge transfer state in crystalline 4-(diisopropylamino)benzonitrile from picoseconds X-ray diffraction. J Am Chem Soc 126:5593–5600
42. Blome C, Tschentscher T, Davaasambuu J, Durand P, Techert S (2005) Femtosecond time-resolved powder diffraction experiments using hard X-ray free-electron lasers. J Syncrotron Radiat 12:812–819
43. Stinton GW, Evans JSO (2007) Parametric Rietveld refinement. J Appl Crystallogr 40:87–95